

The simulation of surface flow dynamics using a flow-path network model

Yumin Chen, Qiming Zhou, Sheng Li, Fanrui Meng, Xiaomei Bi, John P. Wilson, Zisheng Xing, Junyu Qi, Qiang Li & Chengfu Zhang

To cite this article: Yumin Chen, Qiming Zhou, Sheng Li, Fanrui Meng, Xiaomei Bi, John P. Wilson, Zisheng Xing, Junyu Qi, Qiang Li & Chengfu Zhang (2014) The simulation of surface flow dynamics using a flow-path network model, International Journal of Geographical Information Science, 28:11, 2242-2260, DOI: [10.1080/13658816.2014.917312](https://doi.org/10.1080/13658816.2014.917312)

To link to this article: <http://dx.doi.org/10.1080/13658816.2014.917312>



Published online: 22 May 2014.



Submit your article to this journal [↗](#)



Article views: 353



View related articles [↗](#)



View Crossmark data [↗](#)

The simulation of surface flow dynamics using a flow-path network model

Yumin Chen^{a*}, Qiming Zhou^b, Sheng Li^c, Fanrui Meng^d, Xiaomei Bi^a, John P. Wilson^e,
Zisheng Xing^d, Junyu Qi^d, Qiang Li^f and Chengfu Zhang^d

^aSchool of Resource and Environment Science, Wuhan University, Wuhan, Hubei, China; ^bDepartment of Geography, Hong Kong Baptist University, Kowloon, Hong Kong; ^cPotato Research Centre, Fredericton, NB, Canada; ^dFaculty of Forestry and Environmental Management, University of New Brunswick, Fredericton, NB, Canada; ^eSpatial Sciences Institute, University of Southern California, Los Angeles, CA, USA; ^fDepartment of Earth and Environmental Sciences, University of British Columbia, Kelowna, BC, Canada

(Received 12 October 2013; final version received 16 April 2014)

This paper proposes a flow-path network (FPN) model to simulate complex surface flow based on a drainage-constrained triangulated irregular network (TIN). The TIN was constructed using critical points and drainage lines extracted from a digital terrain surface. Runoff generated on the surface was simplified as ‘water volumes’ at constrained random points that were then used as the starting points of flow paths (i.e. flow source points). The flow-path for each ‘water volume’ was constructed by tracing the direction of flow from the flow source point over the TIN surface to the stream system and then to the outlet of the watershed. The FPN was represented by a set of topologically defined one-dimensional line segments and nodes. Hydrologic variables, such as flow velocity and volume, were computed and integrated into the FPN to support dynamic surface flow simulation. A hypothetical rainfall event simulation on a hilly landscape showed that the FPN model was able to simulate the dynamics of surface flow over time. A real-world catchment test demonstrated that flow rates predicted by the FPN model agreed well with field observations. Overall, the FPN model proposed in this study provides a vector-based modeling framework for simulating surface flow dynamics. Further studies are required to enhance the simulations of individual hydrologic processes such as flow generation and overland and channel flows, which were much simplified in this study.

Keywords: flow-path network model; digital terrain analysis; triangulated irregular networks; surface flow

1. Introduction

Classic hydrological models mostly are conceptual or theoretical models, relying on theoretical concepts for specific spatial and temporal units, such that the results lack clear space and time definition (Saint-Venant 1871, Dietrich *et al.* 1993, Turcotte *et al.* 2001). Since the 1980s, the use of GIS to support hydrological modeling has become an important direction of the development of hydrological models. These GIS-supported hydrological models typically use a digital elevation model (DEM) to create a spatial structure for the hydrological processes, so that the simulation of hydrologic processes and the predicted results have a clear spatial footprint.

*Corresponding author. Email: ymchen@whu.edu.cn

Most of hydrological models use a grid-based DEM, because of its simple data structure and ease of implementation with GIS and remote sensing technology (Huggins and Monke 1968, Moore *et al.* 1991, Holmgren 1994, Olivera and Maidment 1999, Bates and De Roo 2000, Jain and Singh 2005). Beven and Kirkby (1979), for example, proposed a topography-based hydrological model (TOPMODEL) that used a square-grid DEM to derive terrain parameters which reflected hydrologic characteristics. However, TOPMODEL does not consider rainfall and evaporation, and thus only partially simulates the key hydrologic processes. The System Hydrologic European (SHE) model proposed by Beven *et al.* (1980), Abbott *et al.* (1986), Bathurst *et al.* (1995), and Refsgaard and Storm (1995) is a typical distributed hydrological model in which the basin is divided into three-dimensional (vertical multi-layer) regular grid in order to combine the model parameters with rainfall data and simulate the hydrologic processes. Another widely used hydrological model is the Soil and Water Assessment Tool (SWAT) model developed by Arnold *et al.* (1994). SWAT model is a semi-distributed hydrological model, which is based on a grid-based DEM to extract hydrological response units (HRUs) with homogeneous hydrologic characteristics.

Despite its popularity, a grid-based DEM has its shortcomings. For example, a grid-based DEM is tied to a single, uniform resolution irrespective of the spatial variability of the hydro-geomorphic processes (Vivoni *et al.* 2005). Therefore, there is high redundancy in a high-resolution DEM and misrepresentation of important hydrologic features, especially linear features, in a low resolution DEM.

A triangulated irregular network (TIN), which consists of areas (facets), lines (edges) and points (vertices or nodes), provides an alternative way of representing the Earth's surface (Jones *et al.* 1990, Dæhlen *et al.* 2001, Kreveld and Silveira 2011, Zhou *et al.* 2011). The TIN can be constructed on critical points (i.e. the so-called turning points) and skeleton lines (e.g. stream and ridge lines) of the terrain surface, so as to retain high densities of points in regions of sharp terrain variations and low densities of points in flat or gently sloping regions (Lee 1991, Heckbert and Garland 1997, Ivanov *et al.* 2004, Chang 2007, Chen and Zhou 2013). For hydrological modeling, several methods have been developed recently to embed drainage networks into a TIN. For instance, Kreveld and Silveira (2011) conflated a TIN structure with a river data set to ensure that the rivers flow along triangular edges in appropriate directions. Zhou and Chen (2011) applied a compound point extraction (CPE) method to construct a drainage-constrained TIN, on which the flow-path can be traced from an arbitrary starting point to the stream system along the steepest-descent direction defined for each facet of the TIN surface.

Several TIN-based models have been developed for hydrologic process simulation. For instance, Palacios-Vélez and Cuevas-Renaud (1992) delineated the ridge and stream lines of a watershed based on TIN models and simulated surface runoff production using interpolated rainfall, soil and river-bed data. Tucker *et al.* (2001) proposed the Channel-Hillslope Integrated Landscape Development (CHILD) model that incorporates a TIN to simulate the landscape evolution resulting from erosion and deposition. Vivoni *et al.* (2005) developed a TIN-based Real-time Integrated Basin Simulator (tRIBS) to predict the surface and subsurface hydrologic response to rainfall.

The TIN-based models have some clear advantages. The TIN-based framework makes it possible to vary spatial resolution as a function of dominant process or landscape position, thus allows accurately capturing the topography, drainage network, floodplain, and soil and land-use features without a significant loss in detail (Vivoni *et al.* 2005). The TIN model also presents a constant slope and aspect for each of its triangular facet and has the ability to support the adaptive resampling of the topographic surface. However, these

advantages come at the price of increased complexity in data structures and flow algorithms. Especially for hydrologic processes, they require not only the preservation of the skeleton lines over a catchment, but also the integration of numerous hydrological parameters that are typically provided in a grid format. Further investigation is also desirable to model the way that various components (e.g. the methods used to construct TIN, to derive flow paths and to compute flow velocity) are combined and used to support a dynamic spatio-temporal surface flow simulation.

For simulating surface flow dynamics, a key challenge is to define the relationship between the magnitude of flow and the corresponding resistance to flow (Djokic and Maidment 1993) at each evaluation unit. In a typical hydrological models (regardless whether it is grid- or TIN-based), the evaluation unit can always be expressed as a facet (rectangular or triangular). This facet-based approach has an inherent disadvantage in hydrological simulation, as there is no determinate way to specify how the flow volume passes from one facet to another. For an arbitrary point on the surface, tracking flow to its source or destination and estimating the passing flow volume are highly influenced by the data structure of DEM and algorithm for flow extraction. Thus, variation in the selection of data structures and algorithms may derive inconsistent outcomes. On the other hand, the scale of hydrological model is determined by the scale of the digital terrain model. Once the scale of a hydrological model changed, a new DEM matching that scale has to be acquired.

In this study, therefore, we propose a flow-path network (FPN) model to simulate surface flow dynamics. The FPN, generated from a drainage-constrained TIN, is composed of nodes and links, forming a tree network of runoff nodes and flow paths. The FPN separates the surface flow simulation process from the underlying DEM so that the impact from the data structure of DEM is reduced. Moreover, the network data structure simplifies the flow simulation from a three-dimensional facet-based to a one-dimensional up- and down-stream process, thus it is readily for the adoption of traditional hydrological methods. The development of FPN is a follow-up of the work by Zhou and Chen (2011), which proposed the CPE method to construct a drainage-constrained TIN. Experiments have been conducted to demonstrate the ability of the FPN for dynamic simulation with a hypothetical data set. The method is then further validated using field measured data obtained from a small watershed.

2. Methodology

The FPN model defines the runoff routing from spatially distributed points to the watershed outlet. Hydrologic simulation with the FPN model includes four steps: (1) construction of the drainage-constrained TIN; (2) definition of the source points of flow paths over the drainage-constrained TIN; (3) delineation of the FPN; and (4) simulation of the surface flow dynamics.

2.1. Construction of the drainage-constrained TIN

In this study, we used the CPE method proposed by Zhou and Chen (2011) to construct the drainage-constrained TIN. Several reports show that the basic topographic characteristics of the terrain surface can be largely preserved when only a relatively small number of critical points (or the 'turning points' of the terrain) are used to generate the TIN (e.g. Lee 1991, Weibel 1992, Li 2008). The CPE method based on the maximum z-tolerance algorithm is used to extract the critical points from regular square-grid-based

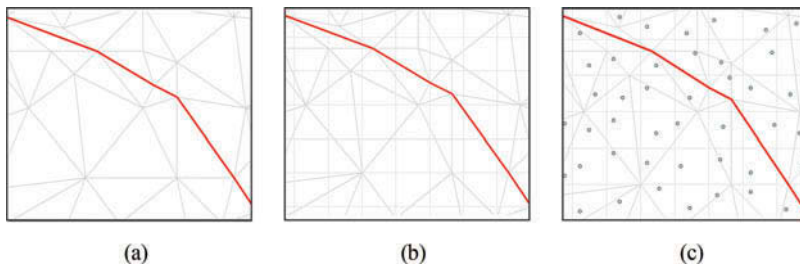


Figure 1. Process of defining the location of 'flow source'. (a) The drainage-constrained TIN structure. (b) The square grids cover the whole TIN. (c) The randomly sampled point as the 'flow source' at every square grid.

DEM. The iterative process is started from an initial TIN with a small number of facets, then elevation defined by the initial TIN will be compared against that of the original DEM and the elevation difference is calculated for each point in the original DEM. The point with the largest elevation difference between the DEM and TIN surface are inserted into the TIN as a critical point to reconstruct a new TIN. The process is repeated until all differences are less than a specified z-tolerance (Heller 1990). Compared with other algorithms, the results show that the CPE algorithm offers the best performance over a series of generalization experiments (Chen *et al.* 2012).

To ensure the proper drainage of the surface flow, the drainage network was extracted from the original DEMs using the simple 'D8' flow routing algorithm (Mark 1984). The drainage network was further generalized using the Douglas–Peucker algorithm (Douglas and Peucker 1973) with a threshold value (e.g. 1, 5 or 10 m) to match the scale of the generated DEM (e.g. 1:10,000, 1:50,000 or 1:100,000, respectively). Then the main streamlines in the extracted drainage network were inserted into the TIN surface as edges, similar to that described by Nelson *et al.* (1999). This way, the main drainage pattern is embedded in the TIN structure (Figure 1(a)).

2.2. Defining the source points of flow paths

Once the drainage-constrained TIN is established, flow paths can be tracked at any location. Source sampling was used to define the starting points for the movement of the 'water volumes'. The flow paths originating from these sources points can then be tracked over the TIN surface.

The common method is to select one sampling point in each triangular facet over a TIN (Jones *et al.* 1990). However, the shape and size of the triangular facets vary tremendously. Many environment variables used in hydrological models, such as rainfall, soil and vegetation, are distributed in a grid format. It is not easy to integrate these grid-format environmental parameters with the TIN structure.

To solve these problems, a square grid covering the entire TIN is created (Figure 1(b)). The resolution of the square grid can be determined by the finest resolution of raster data for the related hydrological and environmental parameters. Then each starting point of a flow path (i.e. 'flow source points') is represented by a randomly located point within that square-grid unit (Figure 1(c)). Runoff generated in each unit is treated as the water volume falling on these representative points, so as to establish the flow paths over the TIN surface.

2.3. Establishing the flow-path network

From the ‘flow source points’, surface flow can be simulated by tracking the movement of flow from the flow source to the outlet.

2.3.1. Computation of slope and aspect of each triangular facet

The movement of the ‘water volumes’ over the TIN surface is assumed to follow the steepest descent of the triangular facets it passes over. So the first step is to compute the slope and aspect of each triangular facet in the TIN. When a drainage-constrained TIN is generated, the slope and aspect are constant for each triangular facet and their values can be determined geometrically as illustrated in Figure 2, following the equations proposed by Zhou *et al.* (2011). The coordinates of the three vertices of a triangle can be specified as $P_1(x_1, y_1, z_1)$, $P_2(x_2, y_2, z_2)$ and $P_3(x_3, y_3, z_3)$, and the facet is formed by a plane as:

$$z = f(x, y) = ax + by + c \tag{1}$$

where a , b and c can be derived as:

$$\left. \begin{aligned} a &= \frac{(y_1 - y_3)(z_1 - z_2) - (y_1 - y_2)(z_1 - z_3)}{(x_1 - x_2)(y_1 - y_3) - (x_1 - x_3)(y_1 - y_2)} \\ b &= \frac{(x_1 - x_2)(z_1 - z_3) - (x_1 - x_3)(z_1 - z_2)}{(x_1 - x_2)(y_1 - y_3) - (x_1 - x_3)(y_1 - y_2)} \\ c &= z_1 - ax_1 - by_1 \end{aligned} \right\} \tag{2}$$

Therefore, the slope (β) and aspect (α) of a triangular facet can be derived as follows:

$$\left. \begin{aligned} \beta &= \arctan \sqrt{a^2 + b^2} \\ \alpha &= \pi - \arctan \frac{b}{a} + \frac{\pi}{2} \frac{a}{|a|} \end{aligned} \right\} \tag{3}$$

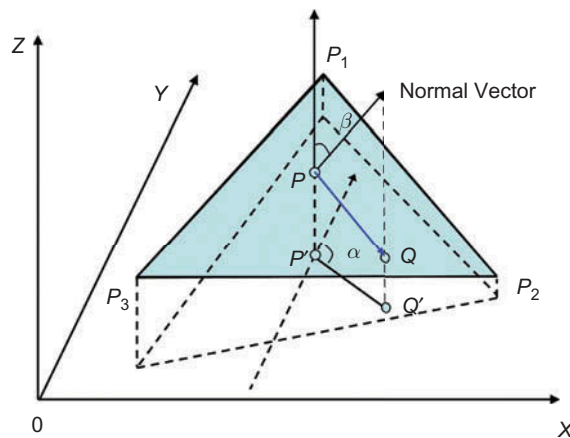


Figure 2. Flow path vector on a triangular facet drawn from the source point.

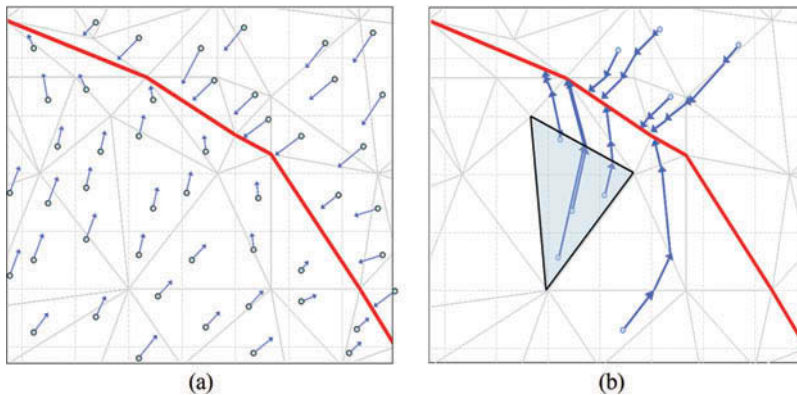


Figure 3. Flow path over the TIN. (a) Flow path vector for each triangular facet at the source points. The direction of an arrow indicates the aspect and the length of each arrow measures the slope of the triangular facet. (b) A flow path (represented by the arrow chains) is formed by tracking the movement of flow.

From the slope and aspect of a triangular facet, we can compute a flow vector (PQ in Figure 2), where point P is the randomly assigned ‘flow source point’ in the triangular facet or on the boundary of the triangular facet.

Such vectors are determined for each computing unit or ‘flow source point’ as illustrated in Figure 3(a).

2.3.2. Vector-based flow path tracking

From the ‘flow source point’, the surface flow direction of each facet is determined using its aspect. The ‘water volume’ moves along the flow direction of the triangular facet toward a downstream triangular facet (Figure 3(b)). When the ‘water volume’ crosses the edge of the facet, it may alter its direction to follow the aspect of the downstream facet. Thus, a ‘flow line’ is formed by tracking the movement of the ‘water volume’ from its source to the ultimate destination (local sink or the catchment outlet).

There are three possible cases for the movement of ‘water volumes’ over the TIN surface:

- (1) If the aspect of the adjacent downstream triangular facet is away from the common edge, the ‘water volume’ flows across the boundary to the adjacent triangular facet, changing direction to the aspect of the adjacent triangular facet.
- (2) If the aspect of the adjacent downstream triangular facet is toward the common edge, the common edge is a ‘valley edge’ and the flow will converge and move along the common edge toward its downstream node.
- (3) If a ‘valley edge’ ends (i.e. there is no connected downstream V-shape edge any more), the flow moves to the triangular facet with the steepest downhill slope. If such a triangular facet is not found, the flow stops.

None of the aforementioned approaches will work, if the adjacent triangular facet or the common edge is level, because the slope and aspect of the triangular facet are zero and it will be difficult to determine the flow direction. Fortunately, a TIN structure has few

critical points in flat areas and the drainage-constrained TIN has the streamlines embedded into the structure. These streamlines are considered as the lowest spots in a local area and they already have predefined flow directions.

2.3.3. *Constructing the topology of the flow-path network*

Each flow-path consists of line segments running across the triangular facets and nodes on the edge of the triangular facet (when flow crosses the edge of the triangular facet, a node is defined). These line segments and nodes are topologically connected. In order to simplify the relationship between line segments, a one-dimensional topological network is defined, which stores only the up-down-stream relations, along with information about the nodes and line segments (connecting two nodes of a triangular facet). The parameters required for hydrological modeling can be derived and topologically linked to the FPN model as the attributes of nodes (e.g. vegetation cover, leaf area index and soil properties) and line segments (e.g. flow velocity, impedance and infiltration rate).

Two tables are used to construct the topology of the FPN, namely the node and the line table (Figure 4). The node table records the node ID, its X, Y and Z coordinates and some terrain characteristics (i.e. land use, soil type). The line table stores the line ID, the start and end node IDs of the line and several hydrologic parameters, such as slope, length and the function for calculating flow velocity (it is determined by flow depth, changing with time).

2.4. *Simulation of spatial-temporal flow dynamics*

Using the FPN as a framework, we can simulate the spatial-temporal dynamics of surface flow. This requires the estimation of cumulative discharge and flow velocity from a flow source point, along the FPN to the basin outlet, which is the process of runoff routing. Runoff routing includes hillslope and channel network routing. In this study, the FPN simplifies the runoff routing moving the runoff along a defined flow-path from high to low elevations, and then to the watershed outlet. It does not distinguish between overland

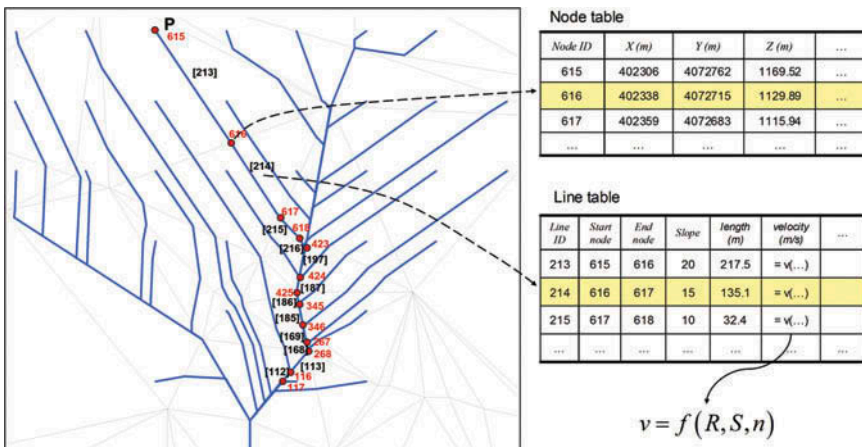


Figure 4. Topology of the flow-path network. The red numbers refer to a node's ID and the black numbers refer to a line segment's ID.

and channel routing. Therefore, the velocity of a line can be derived from the conventional one-dimensional fluvial hydraulics formulae, Manning's equation.

It is assumed that there is no lateral inflow or outflow for a flow path, and the surface flow process can be described using a continuity equation:

$$\frac{\partial Q}{\partial l} + \frac{\partial A}{\partial t} = 0 \quad (4)$$

where A is the flow section area of the channel (m^2), l is the flow length (m) and Q is the cumulative discharge (m^3/s).

The flow velocity along a flow line can be derived from Manning's equation:

$$v = R^{2/3} \cdot S^{1/2} / n \quad (5)$$

where v denotes the flow velocity (m/s), S denotes the slope (m/m), n is Manning's roughness coefficient (dimensionless) which varies with the type of vegetation cover (Thompson 1999) and R denotes the hydraulic radius (m) which can be approximated by the runoff depth h . Then runoff depth h can be computed as follows:

$$h = Q / (vB) \quad (6)$$

where B is the grid cell width (m). In the simulation, Equations (5) and (6) are run iteratively. Initially, an approximate value of runoff depth at time zero h_0 is determined based on the flow rate Q_0 at time zero and the grid size ($B \times B$). The velocity v_0 can then be calculated using Equation (5). The calculated velocity v_0 is used in Equation (6) to determine the flow depth at time step 1, h_1 , which in turn, is used in Equation (5) to determine flow velocity at time step 1, v_1 , and so on until the end of the simulation period.

The runoff travel time t is determined by:

$$t = \frac{L}{v} = \frac{nL}{R^{2/3}S^{1/2}} \quad (7)$$

where t is the travel time of runoff through the line segment (s), L is the length of the line segment (over each triangular facet) (m) and v is flow velocity (m/s).

With each time step, the 'water volumes' have moved a certain distance (depending on slope and runoff depth), and all 'water volumes' within a computation unit are merged after each iteration. The runoff flow is determined by the cumulative discharge (m^3/s) through the cell (i.e. the computation unit) that is determined by summing up the upstream flow contributions from all flow lines in each respective time interval.

3. Model verification and validation

Two tests were conducted to verify and validate the proposed FPN model. In the first test, the FPN was used to simulate surface flow in a hilly landscape after a hypothetical rainfall event to verify the responsive surface flow dynamics in real time. In the second test, the FPN was applied to a small catchment in northern New Brunswick, Canada, and validated against field observations.

3.1. Verification of real-time simulation of a runoff event

A high-resolution DEM derived from a topographic map drawn at a scale of 1:10,000 and composed of 1091×892 grid cells with a 5-m spatial resolution was used (Figure 5(a)). The landscape is topographically complex, with a very high density of erosion features such as gullies so that the topographic control on the drainage pattern can be clearly visualized. Prior to running the FPN, the DEM was pre-processed to fill local pits and sinks using ArcGIS 9.3 (Environmental Systems Research Institute, Inc.; www.esri.com).

For the purpose of verifying the real-time surface flow dynamics, a hypothetical rainfall event was used in this first test. As illustrated in Figure 6, rainfall intensity (indicated by raindrop density in the map) varied in time and space in this hypothetical event. The center of the rainfall began on the low-right corner of the test area, then moved to the center with higher density, and finally disappeared from the upper-left corner.

The hypothetical rainfall event lasted 1200 s (20 min) with an average total rainfall of 12 mm across the test area. In order to simplify the computation, it was assumed that

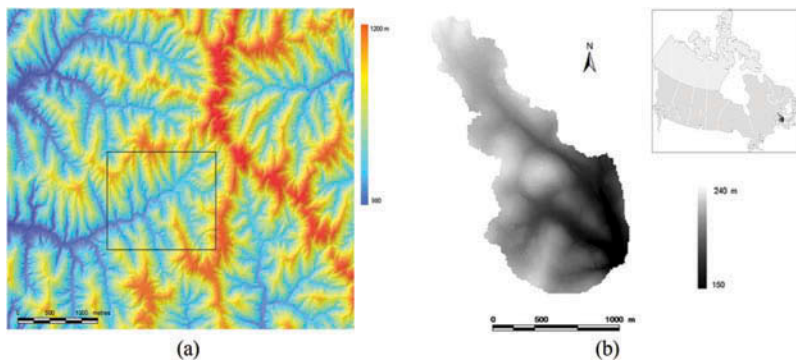


Figure 5. DEM utilized for the experiments (a) the test DEM used for the hypothetical rainfall simulation (1091×892 cells, 5 m cell size). (b) DEM of the BBW used for the real-world catchment test (942×1284 cells, 5 m cell size).

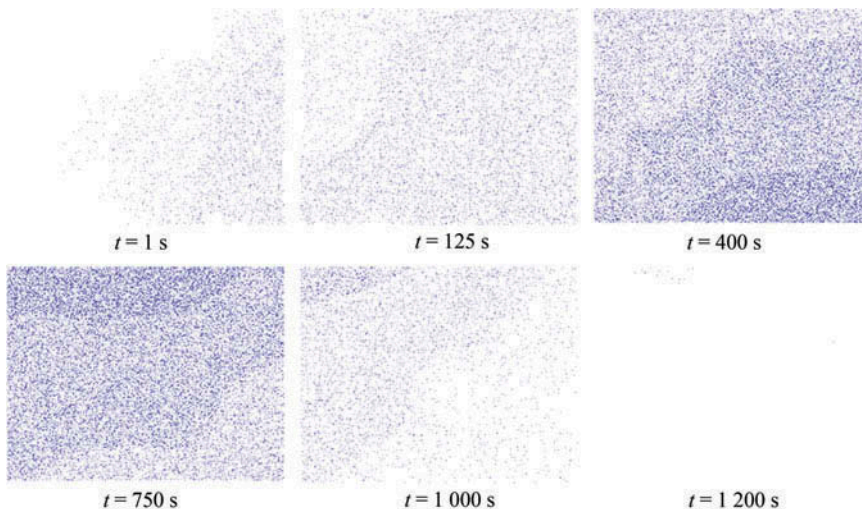


Figure 6. A simulated hypothetical rainfall event.

infiltration and other losses of water were negligible (such as might occur after a long wet period) so that all raindrops were turned into surface runoff.

The surface flow dynamics was simulated with the FPN as described in the methodology section. The drainage network extracted from the original DEM using ArcGIS 9.3 with the simple D8 flow routing algorithm was embedded into the TIN structure as edges. A TIN was generated using the critical points and the drainage line edges. Slope and aspect for each triangular facet were calculated based on Equations (2) and (3). A 90-m resolution grid was used to establish the spatial unit and a random point was generated in each grid cell. Runoff generated from rainfall was initiated from these flow source points along the aspect of the facet or valley edges downstream to the watershed outlet. The flow velocity was computed for each line segment using Equations (5) and (6). The values for Manning's n , tabulated according to factors that affect roughness, were taken from Thompson (1999). The simulation was conducted at a time interval of 1 s. Runoff was treated as discrete 'water volumes' generated on each flow source point at each time interval. The position of each 'water volume' moving downstream along its flow-path was dynamically computed at each time interval thereafter using Equation (7). The flow rate at each node was also calculated (using the flow velocity multiplied by the cross-sectional area) at each time interval. Therefore, time series maps of flow pattern can be produced.

3.2. A real-world catchment test

For the real-world catchment test, the Black Brook watershed (BBW) in northwestern New Brunswick in Canada was used (Figure 5(b)). The watershed is located between 47°05' and 47°09' N and between 67°43' and 67°48' W. Elevation in BBW ranges from 150 to 240 m above mean sea level. The total area of the watershed is approximately 13 km². The monthly average precipitation ranged from a low of 64.6 mm in February to a high of 111.6 mm in July with a mean value of 91 mm (Yang *et al.* 2009). Most of the BBW consists of undulating to gently rolling landforms with slopes of 1–6% in the upper portions, slopes of 4–9% in the central parts and slopes of 5–16% in the strongly rolling lower positions. Long-term monitoring stations for weather, surface and ground water were established in the BBW in the early 1990s and land use and management practices in each field in the BBW have been recorded since this time as well. These data have been used in many watershed and agri-environmental related studies (e.g. Yang *et al.* 2009). The DEM used for this test was composed of 942 × 1284 grid cells with a 5-m spatial resolution and was produced from raw 1-m density elevation data obtained using the light detection and ranging (lidar) technology. The basic input data used in this test are summarized in Table 1 and more detailed descriptions of the data collection can be found in Yang *et al.* (2009).

As a first field test of the FPN model, the purpose of this validation exercise is to evaluate the runoff routing simulation in FPN. The generation of runoff was simulated using the SWAT model. For comparison, runoff routing was simulated using both the SWAT and FPN models. The simulation in SWAT followed the procedure described in detail by Yang *et al.* (2009). Parameters for the FPN method were obtained as follows: (1) the threshold used for the maximum z-tolerance for determining the critical points was 0.7 m; (2) the spatial unit was a square grid with a 30 m resolution; and (3) the Manning's roughness coefficients used in Equations (5) and (7) were determined based on the land-use types (Table 1) and the values proposed by Thompson (1999). The models were run for 2001 (given the readily available published data). Since only daily input data were available, the two models were run using a daily time step and the validation was conducted by comparing the model-predicted to the field-observed daily flow rate at the watershed outlet.

Table 1. Summary of input data used for the simulations in the Black Brook watershed.

Input data	Description
DEM	Generated from lidar data obtained at about 1-m density
Land use	Potato 32% Barley 23% Forest 22% Residents 5.3% Others 11.6% Others agriculture land 6.1%
Climate	Wind speed Solar radiation Daily precipitation Relative humidity Maximum and minimum air temperature
Soil	AAFC detailed soil survey map

The observed daily flow rate (which combined surface runoff and baseflow) at the outlet of the BBW in 2001 was measured using a gauging station established in 1992. It should be noted that as the FPN only simulated the surface runoff, the total flow rate was calculated by adding the FPN predicted surface runoff flow rate to the baseflow rate calculated using the procedure proposed by Zhang *et al.* (2012). For comparison purposes, the same procedure was followed for the SWAT predicted total flow rate.

Three statistical indicators, the Nash efficiency (E) (Nash and Sutcliffe 1970), correlation coefficient (R) and the balance coefficient (B), were used to evaluate the performance of the model as follows:

$$E = 1 - \frac{\sum_{t=1}^T (Q_o^t - Q_m^t)^2}{\sum_{t=1}^T (Q_o^t - \overline{Q_o})^2} \quad (8)$$

$$R = \frac{\sum_{i=1}^n (Q_m^t - \overline{Q_m})(Q_o^t - \overline{Q_o})}{\sqrt{\sum_{i=1}^n (Q_m^t - \overline{Q_m})^2 \sum_{i=1}^n (Q_o^t - \overline{Q_o})^2}} \quad (9)$$

$$B = \frac{\sum_{t=1}^T Q_o^t}{\sum_{t=1}^T Q_m^t} \quad (10)$$

where Q_o is the observed discharge, Q_m is the modeled discharge and t denotes time. E and R measure the model accuracy and precision, while B measures the potential bias of the model. For all three indicators, a value close to 1 indicates better model performance.

4. Results

4.1. Verification of real-time simulation of a runoff event

Figure 7 shows the FPN simulated surface flow rate at different times corresponding to the rainfall pattern shown in Figure 6. In the first second, rainfall started from the east side of the test area (Figure 6) at low intensity and correspondingly, runoff appeared in the east part of test area immediately due to the zero infiltration assumption (Figure 7). After 125 s, rainfall covered the entire test area and the intensity increased slightly (Figure 6). Correspondingly, water drops appeared in the whole test area and the density of water drops increased (Figure 7). In addition, as a result of flow accumulation and convergence, major stream lines can be visualized, but flow rate in all streams is low (blue in color). Rainfall intensity continuously increased and the center of rainfall moved toward the northwest after that time (Figure 6). This was reflected in the pattern and density of water drops on the $t = 400$ s and $t = 750$ s maps (Figure 7). More importantly, due to flow accumulation, the flow rate increased along the stream as indicated by the change in color of the stream on the maps. After 400 s, the upper-stream segments were blue ($0-0.25$ m³/s) or green ($0.25-0.5$ m³/s), while the lower-stream segments have changed to yellow ($0.5-2.5$ m³/s). After 750 s, a part of the lower stream changed to red (>2.5 m³/s). After 935 s, the rainfall intensity decreased substantially (Figure 6) as reflected by the lower density of water drops (Figure 7). However, the main lower-stream remained red in color (>2.5 m³/s). This is due to the lag in flow accumulation (it took time for water to flow from their flow source points to the stream). After 1200 s, the rain has almost stopped and many upper-streams had no flow any more (i.e. they had disappeared from the map in Figure 6). It took a long time for the runoff to drain out, again due to the lag in flow accumulation.

The variations of flow with space and time can also be demonstrated with hydrographs at different points in the DEM. Figure 8 shows that the hydrographs predicted by the FPN at three locations indicated with the red circles in Figure 7 (from left to right, lower-stream, intermediate and upper-stream points). At first, the flow rate at all three locations was low, a direct reflection of in-situ runoff generation. Due to flow accumulation, the flow rate increased along the stream over time. The flow rate at the upper-stream point featured a

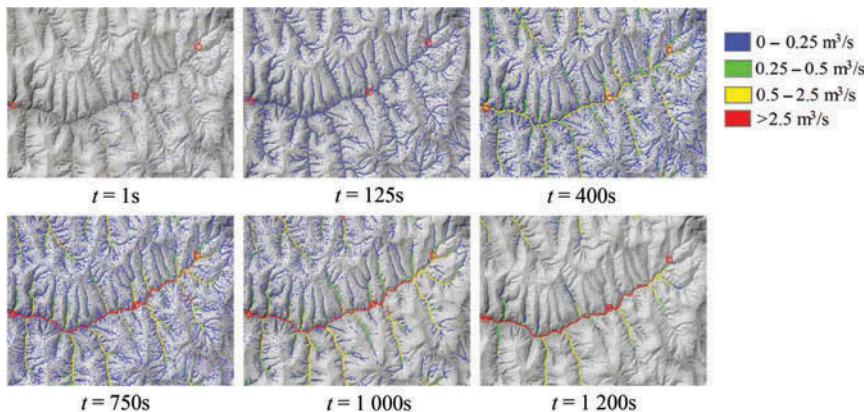


Figure 7. Surface flow simulated at different times for a hypothetical rainfall event. The three red circles indicate reference points at high, intermediate and low elevations along the main stream, for which the hydrographs as shown were reproduced in Figure 8.

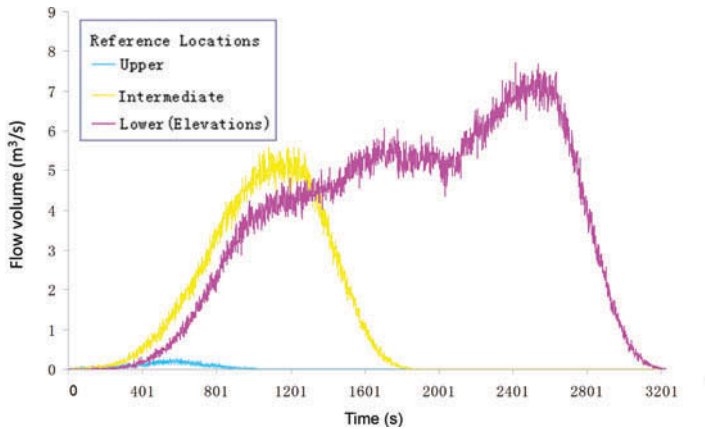


Figure 8. Hydrograph showing surface flow volumes simulated at three reference locations (see Figure 7) at different times.

flat and low peak and stopped at about $t = 900$ s. This is because its drainage area was small and the flow lengths were short. At the intermediate point, the flow rate curve rose up at about $t = 300$ s and featured a high peak centered near $t = 1200$ s, when the rainfall actually stopped. It took another 600 s for the flow to subside and water to drain out from this point. At the lower-stream point, the flow rate curve grew more slowly than for the intermediate point curve. However, the lower-stream curve sustained at high flow rates from about $t = 1000$ s to about $t = 2600$ s, indicating a longer period of flow accumulation due to its larger drainage area. The patterns shown in these graphs comply with what we expected, based on knowledge of the hydrologic processes and therefore, the ability of the FPN for simulating real-time surface flow dynamics is considered verified.

4.2. Validation of the FPN in BBW

With a z-tolerance threshold of 0.7 m, a total of 7621 critical points were extracted from the original 5 m DEM of the BBW (Figure 9(a)). After imbedding the extracted drainage network, the drainage-constrained TIN contains a total of 18,307 triangular facets, which

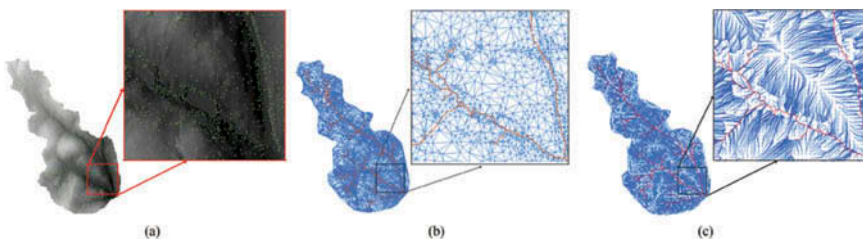


Figure 9. The process of applications of the flow-path network model in BBW. (a) The Critical points of the high-resolution DEM were extracted by the maximum z-tolerance algorithm. (b) The drainage-constrained TIN structure of the DEM. The blue lines denote the stream lines that are embedded in the TIN structure. (c) The flow paths tracked over a TIN surface and the resulting flow-path network structure. The red lines denote the stream lines; the blue lines denote the flow path lines.

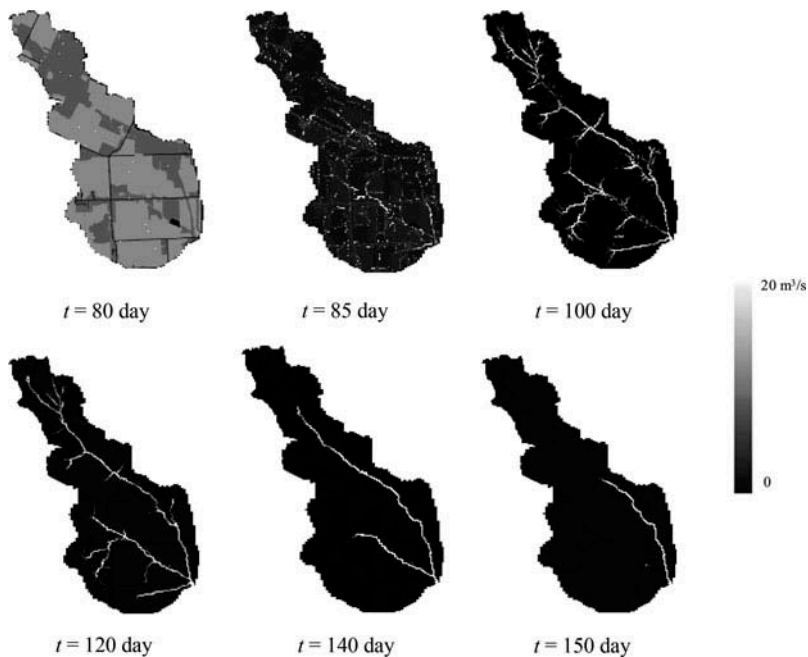


Figure 10. Surface flow simulated for real rainfall event at BBW basin at six representative dates.

covered 710 m^2 on average (Figure 9(b)). The established FPN had a total of 16,254 line segments (Figure 9(c)).

Figure 10 shows surface flow simulated for the BBW at different times. From day 80 to day 150, flow was generated unevenly across the surface and the flow rate varied along different parts of the surface due to flow accumulation. Thereafter, the outline of the stream was formed. Then the upper-stream segments started disappearing and on the flows on the lower-stream segments decreased. By day 150, many of the upper-stream reaches had disappeared.

Figure 11 show the observed and simulated daily flow discharge (with both SWAT and FPN) at the BBW outlet in 2001. Both models seem to be able to predict the major pattern of the flow discharge at the watershed outlet. However, the observed data appeared to have fewer and lower runoff peaks, especially during the snowmelt period in early spring (i.e. from day 90 to 140 or thereabouts). Comparing the two models, the FPN prediction appeared to agree with the observed data slightly better than SWAT. This difference is consistent with the values of the three statistical indicators (Table 2). For example, the FPN produced slightly better results in terms of the Nash efficiency coefficient (E), which was 20% higher than the results for the SWAT model. A similar result is shown for the balance coefficient (B) since the values obtained with the FPN were much closer to 1 than the equivalent values obtained with the SWAT model. The correlation coefficient (R) values for the two methods provided very similar results, given differences of less than 10%. For both models, the predicted peaks of flow were higher than the measured values. One potential reason for this outcome could be that the high water retention capacity in forested areas was not considered during the calculation of surface runoff, which is not related to the routing process. In addition, the subsurface flow and groundwater flows were not considered in either model.

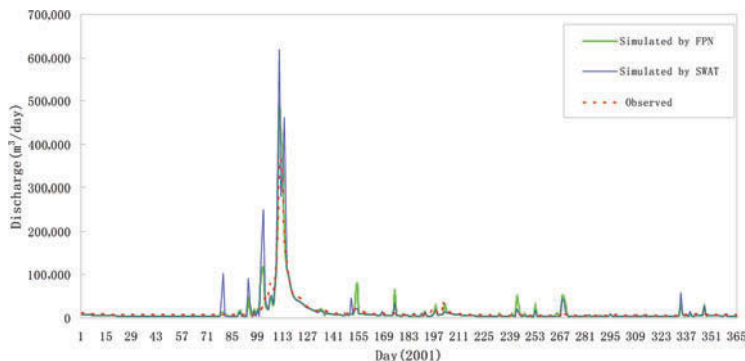


Figure 11. Comparison between observed and simulated discharge at the outlet of the BBW basin in 2001 using the SWAT and FPN.

Table 2. Statistical indicators used to evaluate the performance of the SWAT and FPM in predicting the flow discharge at the outlet of the Black Brook watershed.

Runoff method	Nash efficiency coefficient (E)	Correlation coefficient (R)	Balance coefficient (B)
SWAT model	0.416	0.873	0.964
Flow path model	0.523	0.885	0.994

5. Discussion

The proposed FPN model simplifies the complex three-dimensional water flow distribution over a terrain surface to a one-dimensional up-down relationship, and we attempted to reconstruct the surface flow pattern by incorporating Manning's equation. Through these experiments, the topological FPN model demonstrates two advantages linked to the one-dimensional representation and the ability to support multi-scale real-time simulations.

5.1. Simplifying the three-dimensional surface to a one-dimensional representation for dynamics simulations

The FPN developed in this study constructs a topologically connected stream network for predicting hydrologic flow paths. The model stores nodes and line segments and thereby converts complicated three-dimensional terrain surface flow paths (see Wilson *et al.* (2008) for several examples of such approaches) into a simple one-dimensional relation. The flow-paths have both topological integrity and multi-scale characteristics. This linear topological data structure gives the model the ability to incorporate different resolutions (big and small facets) in one data set based on the importance of data (critical points). Therefore, it simplifies a three-dimensional hydrological process to a one-dimensional representation and makes the upscaling and downscaling of the core data easier.

The simplification of modeling structure makes the surface flow simulation more flexible. Since the FPN modeling can start the simulation from any given points, so essentially any point on the terrain surface can be used to construct a vector-based flow path and to be connected to the final outlet point. In addition, conventional hydrology functions and formulae, which are often built on simple structures (e.g. Manning's

equation for a line segment), then can be easily incorporated into the topological FPN model.

5.2. Ability to support multi-scale real-time simulations

The FPN model relies on points and lines such that a variety of other important parameters can be integrated into the node (vegetation type and cover, soil thickness and dynamic underlying surface characteristics) and line structures (slope, flow length and velocity). The topological FPN is considered valuable because it can be used to estimate water movement in time and space. The simulation can be conducted at any time interval and the position of each 'water volume' along its flow path and the flow rate at each node can be dynamically computed at each time interval. Therefore, time series maps of flow pattern can be produced. The real-time simulation of a runoff event showed that the FPN is capable of simulating real-time surface flow dynamics.

In the traditional hydrological models, the scale of the digital terrain model determines the scale of the hydrological modeling. In order to simulate multi-scale phenomena, multiple DEMs at the scales of interest need to be created. For the FPN model, the TIN surface is used as a base on which the simulation is initiated from any given points. Thus the separation of process simulation units from their underlying digital terrain model makes it possible to achieve the multi-scale hydrological models on the same TIN surface. When a multi-scale analysis is needed, the FPN offers flexibility in (1) using a scale-adaptive TIN representation (e.g. Chen and Zhou 2013), (2) varying the distribution and density of 'source points' or (3) combining both above options.

5.3. Limitations and future enhancements

As demonstrated in this study, the FPN offers several advantages for hydrologic modeling. However, it also presents some challenges for further development and application. For example, various common database optimization and management techniques such as quad trees and compression may be applied to the node and line tables to represent the topological relations, so that data storage and retrieval performance can be enhanced. Many efforts have been made to improve the computation efficiency. For example, Liu *et al.* (2014) utilized parallel computing to enhance the performance of the model. Techniques such as parallel computing can be incorporated into the model structure to further increase the efficiency. Similarly, further work is required to enhance the simulations of individual hydrologic processes such as flow generation and overland and channel flows, thereby to improve FPN's capability and applicability. Finally, the impact of environment variables on the outcome of the FPN model for flow prediction is also a subject for further investigation.

6. Conclusions

In this study, we proposed an FPN model for surface flow modeling based on a drainage-constrained TIN. The FPN model has the advantages of representing water movement with a series of simple one-dimensional relations and integrating environmental variables for real-time simulation.

The ability of the FPN was demonstrated by a hypothetical rainfall-runoff case for the support real-time simulation of surface flow. A real-world case study has shown that the FPN predicted daily runoff discharge at a watershed outlet agreed well with field

measurements. The accuracy of the FPN predictions was comparable to or slightly better than that of the SWAT model predictions. It would be logical to compare the output from the proposed network model to an established TIN-based model, such as tRIBS model. However, implementing a TIN-based model would have to deal with potential data conversion issues that are out of scope of this study and subject to more extensive studies in the future. It is recognized that further investigation is needed to enhance the ability of the FPN for the simulation of various hydrological processes. Nevertheless, our work has shown that the FPN is capable of delivering encouraging outcomes for real-time surface flow process simulation.

Acknowledgements

The research was supported by grants from National High Technology Research and Development Program of China (Project No. 2013AA122302), National Nature Science Foundation of China (Project No. 41171347), Hong Kong Research Grants Council General Research Fund Grant (HKBU 203913), Hong Kong Baptist University Faculty Research Grant (FRG1/12-13/070) and Agriculture and Agri-Food Canada (Project 1145).

References

- Abbott, M.B., *et al.*, 1986. An introduction to the European hydrological system – système hydrologique Européen, ‘SHE’, 1: history and philosophy of a physically-based, distributed modelling system. *Journal of Hydrology*, 87, 45–59. doi:10.1016/0022-1694(86)90114-9.
- Arnold, J.G., *et al.*, 1994. *SWAT – soil and water assessment tool – user manual*. Grassland, TX: Agricultural Research Service, Soil and Water Research Laboratory, US Department of Agriculture.
- Bates, P.D. and De Roo, A.P.J., 2000. A simple raster-based model for flood inundation simulation. *Journal of Hydrology*, 236, 54–77. doi:10.1016/S0022-1694(00)00278-X.
- Bathurst, J.C., Wicks, J.M., and O’Connell, P.E., 1995. The SHE/SHESED basin scale water flow and sediment transport modelling system. In: V.P. Singh, eds. *Computer models of watershed hydrology*. Highlands Ranch, CO: Water Resources Publication, 563–594.
- Beven, K.J. and Kirkby, M.J., 1979. A physically based, variable contributing area model of basin hydrology / un modèle à base physique de zone d’appel variable de l’hydrologie du bassin versant. *Hydrological Sciences Bulletin*, 24, 43–69. doi:10.1080/02626667909491834.
- Beven, K.J., Warren, R., and Zaoui, J., 1980. SHE: towards a methodology for physically-based distributed forecasting in hydrology. *Hydrological Forecasting* (IAHS Publication), 129, 133–137.
- Chang, K., 2007. *Introduction to geographic information systems*. 4th ed. New York: McGraw-Hill. 450.
- Chen, Y. and Zhou, Q., 2013. A scale-adaptive DEM for multi-scale terrain analysis. *International Journal of Geographical Information Science*, 27 (7), 1329–1348. doi:10.1080/13658816.2012.739690.
- Chen, Y., *et al.*, 2012. Comparison of drainage-constrained methods for DEM generalization. *Computers & Geosciences*, 48, 41–49. doi:10.1016/j.cageo.2012.05.002.
- Dæhlen, M., Fimland, M., and Hjelle, Ø., 2001. A triangle-based carrier for geographical data. In: P.J. Halls, ed. *Innovations in GIS 8: spatial information and the environment*. New York: Taylor & Francis, 105–120.
- Dietrich, W.E., *et al.*, 1993. Analysis of erosion thresholds, channel networks, and landscape morphology using a digital terrain model. *The Journal of Geology*, 101, 259–278. doi:10.1086/648220.
- Djokic, D. and Maidment, D.R., 1993. Application of GIS network routines for water flow and transport. *Journal of Water Resources Planning and Management*, 119 (2), 229–245. doi:10.1061/(ASCE)0733-9496(1993)119:2(229).
- Douglas, D.H. and Peucker, T.K., 1973. Algorithms for the reduction of the number of points required to represent a digitized line or its caricature. *Cartographica: the International Journal*

- for *Geographic Information and Geovisualization*, 10 (2), 112–122. doi:10.3138/FM57-6770-U75U-7727.
- Heckbert, P.S. and Garland, M., 1997. *Survey of polygonal surface simplification algorithms*. Sigggraph 97 Course Notes, no. 25. New York: ACM Press.
- Heller, M., 1990. Triangulation algorithms for adaptive terrain modelling. In: K.E. Brassel and H. Kishimoto, eds. *Proceedings of the 4th international symposium on spatial data handling*, vol. 1, 23–27 July, Zürich. 163–174.
- Holmgren, P., 1994. Multiple flow direction algorithms for runoff modelling in grid based elevation models: an empirical evaluation. *Hydrological Processes*, 8, 327–334. doi:10.1002/hyp.3360080405.
- Huggins, L.F. and Monke, E.J., 1968. A mathematical model for simulating the hydrologic response of a watershed. *Water Resources Research*, 4 (3), 529–539. doi:10.1029/WR004i003p00529.
- Ivanov, V.Y., et al., 2004. Catchment hydrologic response with a fully distributed triangulated irregular network model. *Water Resources Researcher*, 40, W11102. doi:10.1029/2004WR003218.
- Jain, M.K. and Singh, V.P., 2005. DEM-based modelling of surface runoff using diffusion wave equation. *Journal of Hydrology*, 302, 107–126. doi:10.1016/j.jhydrol.2004.06.042.
- Jones, N.L., Wright, S.G., and Maidment, D.R., 1990. Watershed delineation with triangle-based terrain models. *Journal of Hydraulic Engineering*, 116 (10), 1232–1251. doi:10.1061/(ASCE)0733-9429(1990)116:10(1232).
- Kreveld, M.V. and Silveira, R.I., 2011. Embedding rivers in triangulated irregular networks with linear programming. *International Journal of Geographical Information Science*, 25 (4), 615–631. doi:10.1080/13658816.2010.488240.
- Lee, J., 1991. Comparison of existing methods for building triangular irregular network models of terrain from grid digital elevation models. *International Journal of Geographical Information Systems*, 5 (3), 267–285. doi:10.1080/02693799108927855.
- Li, Z., 2008. Multi-scale digital terrain modelling and analysis. In: Q. Zhou, B. Lees, and G. Tang, eds. *Advances in digital terrain analysis*. Berlin: Springer, 59–83.
- Liu, J., et al., 2014. A layered approach to parallel computing for spatially distributed hydrological modeling. *Environmental Modelling & Software*, 51, 221–227. doi:10.1016/j.envsoft.2013.10.005.
- Mark, D.M., 1984. Part 4: mathematical, algorithmic and data structure issues: automated detection of drainage networks from digital elevation models. *Cartographica: the International Journal for Geographic Information and Geovisualization*, 21 (2), 168–178. doi:10.3138/10LM-4435-6310-251R.
- Moore, I.D., Grayson, R.B., and Ladson, A.R., 1991. Digital terrain modelling: a review of hydrological, geomorphological, and biological applications. *Hydrological Processes*, 5, 3–30. doi:10.1002/hyp.3360050103.
- Nash, J.E. and Sutcliffe, J.V., 1970. River flow forecasting through conceptual models part I – a discussion of principles. *Journal of Hydrology*, 10 (3), 282–290. doi:10.1016/0022-1694(70)90255-6.
- Nelson, E.J., Jones, N.L., and Berrett, R.J., 1999. Adaptive tessellation method for creating tins from GIS data. *Journal of Hydrologic Engineering*, 4 (1), 2–9. doi:10.1061/(ASCE)1084-0699(1999)4:1(2).
- Olivera, F. and Maidment, D., 1999. Geographic information systems(gis)-based spatially distributed model for runoff routing. *Water Resources Research*, 35 (4), 1155–1164. doi:10.1029/1998WR900104.
- Palacios-Vélez, O.L. and Cuevas-Renaud, B., 1992. SHIFT: a distributed runoff model using irregular triangular facets. *Journal of Hydrology*, 134, 35–55. doi:10.1016/0022-1694(92)90027-S.
- Refsgaard, J.C. and Storm, B., 1995. MIKE SHE. In: V.P. Singh, ed. *Computer models of watershed hydrology*. Highlands Ranch, CO: Water Resources Publication, 809–846.
- Saint-Venant de, B., 1871. Theory of unsteady water flow, with application to river floods and to propagation of tides in river channels. *French Academy of Science*, 73 (148-154), 237–240.
- Thompson, S.A., 1999. *Hydrology for water management*. Rotterdam: A Balkema.
- Tucker, G.E., et al., 2001. The channel-hillslope integrated landscape development (CHILD) model. In: R.S. Harmon and W. Doe, eds. *Landscape erosion and evolution modelling*. Dordrecht: Kluwer Academic/Plenum Publishers, 349–388.

- Turcotte, R., *et al.*, 2001. Determination of the drainage structure of a watershed using a digital elevation model and a digital river and lake network. *Journal of Hydrology*, 240, 225–242. doi:10.1016/S0022-1694(00)00342-5.
- Vivoni, E.R., *et al.*, 2005. Embedding landscape processes into triangulated terrain models. *International Journal of Geographical Information Science*, 19 (4), 429–457. doi:10.1080/13658810512331325111.
- Weibel, R., 1992. Models and experiments for adaptive computer-assisted terrain generalization. *Cartography and Geographic Information Science*, 19 (3), 133–153. doi:10.1559/152304092783762317.
- Wilson, J.P., *et al.*, 2008. Water in the landscape: a review of contemporary flow routing algorithms. In: Q. Zhou, B. Lees, and G. Tang, eds. *Advances in digital terrain analysis*. Berlin: Springer, 213–236.
- Yang, Q., *et al.*, 2009. Assessing the impacts of flow diversion terraces on stream water and sediment yields at a watershed level using SWAT model. *Agriculture Ecosystems and Environment*, 132 (1–2), 23–31. doi:10.1016/j.agee.2009.02.012.
- Zhang, R., *et al.*, 2012. Baseflow separation in a small watershed in New Brunswick, Canada, using a recursive digital filter calibrated with the conductivity mass balance method. *Hydrological Processing*, 27 (18), 2659–2665. doi:10.1002/hyp.9417.
- Zhou, Q. and Chen, Y., 2011. Generalization of DEM for terrain analysis using a compound method. *ISPRS Journal of Photogrammetry and Remote Sensing*, 66 (1), 38–45. doi:10.1016/j.isprsjprs.2010.08.005.
- Zhou, Q., Pilesjö, P., and Chen, Y., 2011. Estimating surface flow-paths on a digital elevation model using a triangular facet network. *Water Resources Researcher*, 47, W07522. doi:10.1029/2010WR009961.W07522.